Disintegration Mechanism and Hydrogeochemical Processes of Red-Bed Soft Rock Under Drying-Wetting Cycle

Kai Huang
Hefei University of Technology https://orcid.org/0000-0002-5326-9842
Bo Kang
Hefei University of Technology
Fusheng Zha (geozha@hfut.edu.cn)
Hefei University of Technology
Yunfeng Li
China Geological Survey Nanjing Center: Nanjing Geological Survey Center
Qing Zhang
China Geological Survey Nanjing Center: Nanjing Geological Survey Center
Chengfu Chu
Hefei University of Technology

Research Article

Keywords: Red-bed argillaceous siltstone, Disintegration mechanism, Drying-wetting cycles, Hydrogeochemical process, Microstructural analysis

Posted Date: May 4th, 2021

DOI: https://doi.org/10.21203/rs.3.rs-444708/v1

Disintegration mechanism and hydrogeochemical processes of red-bed soft rock under drying-wetting cycle

Kai Huang[1], Bo Kang[1], Fusheng Zha[1*], Yunfeng Li[2], Qing Zhang[2], Chengfu Chu[1]

[1]*School of Resource and Environmental Engineering, Hefei University of Technology, Hefei, 230009, China*

[2]*Nanjing Geological Survey Center, China Geological Survey, Nanjing, JiangSu 210016, China*

***Corresponding author**

Prof. Fusheng Zha

School of Resource and Environmental Engineering, Hefei University of Technology

No.193, Tunxi Road, Hefei, 230009

P.R. China

Email: geozha@hfut.edu.cn

Tel: +86 551 62901523

Mobile: +86 13696533099

Fax: +86 55162901524

Abstract: Red-bed soft rock in the drawdown area on bank slopes of landslide easily disintegrates upon exposure to water, and its properties experience comprehensive deterioration, which will cause bank slope instability. To better study disintegration mechanism of the red-bed soft rock, a series of laboratory tests were conducted in this paper to investigate the disintegration characteristics, durability and hydrogeochemical process of red-bed argillaceous siltstone under drying-wetting cyclic conditions. Experimental results showed that, with increasing number of drying-wetting cycles, red-bed argillaceous siltstone gradually disintegrated, from initial appearing the cracks on the surface of the samples to large particles gradually breaking up into small fragments. Significant changes in grain size distribution, and the durability index of the samples progressively decreased. Microstructural analysis showed that the size and distribution of pores and cracks in the sample surface significantly increased, such that the sample surface became disordered and complicated. Notable changed in concentrations of ions in the soaking solutions indicated continuous mineral dissolution and loss during the cyclic drying-wetting. Based on the results obtained from the experiment, it is concluded that the disintegration of samples undergoing drying-wetting cycles was the result of the synergistic action of water and temperature. To be specific, the dissolution of calcite, albite, gypsum, montmorillonite and kaolinite during the wetting procedure, which promotes the decrease in mineral content and increases in pores and cracks. The increases in temperature and the dehydration shrinkage of sample during the drying procedure accelerated the disintegration of the samples.

Keywords: Red-bed argillaceous siltstone; Disintegration mechanism; Drying-wetting

cycles; Hydrogeochemical process, Microstructural analysis.

1 Introduction

Red-bed soft rock is a sedimentary rock of the Triassic, Jurassic, and Cretaceous systems, with red, purple and dark red colors, and it is a typical soft rock, which including sandstone, siltstone, shale, and mudstone. In addition, red-bed soft rock is a kind of multiphase composite with microscopic pores and cracks result in these rocks being highly vulnerable to the effects of water. Resulting in disintegration with water, which can severely affects the stability of rock masses and result in problems in engineering construction (Molina et al. 2011). Additionally, red-bed soft rock is widely distributed across the globe, and is often encountered in major engineering construction projects (Rincon et al. 2016). Therefore, the disintegration characteristics of red-bed soft rock are worthy of thorough investigation, and have attracted extensive attention during the past decade (Kurlenya and Oparin 1996; Doostmohammadi et al. 2009; Selen et al. 2019).

Disintegration is a physical and chemical weathering process that is affected by many factors. Phienwej (1995) found that disintegration was caused mainly by changes in the water content of rock. Similar results were found by Newman (1983) and Liu et al. (2000), the results showed that disintegration of mudstone was caused by the presence of water, which reduced the degree of cementation among mineral particles. Youn and Tonon (2010) considered that the disintegration is the structural degradation of an intact mass into smaller particles due to a change in water content. Zhang et al. (2012) and Liang (2016) indicated that high temperature accelerated the disintegration

of mudstone during the tests. In addition, as the significant impact parameters in disintegration, the mineral composition and microstructure of rock have been widely investigated in previous studies (Huang et al., 2020; Hua et al., 2015; Ghobadi et al. 2014; Hajdarwish et al. 2013; Dhakal et al. 2002). According to the studies conducted by Deng et al. (2016) and Pham et al. (2007), the propagation of macro-cracks caused by water was closely related to the material composition of mudstone. Gökceoğlu et al. (2000) and Pejon et al. (1998) investigated the influence of mineralogical composition on durability. The experiments proved that as the amount of clay minerals gradually increases, the durability of the soft rock decreased. Tests conducted by Bryson et al. (2012), Weng and Li (2012) and Cantón et al. (2001) also found that increases in cracks and clay minerals resulted in a more complete disintegration of rocks.

Water-weakening effects on soft rocks have been a major research topic in rock engineering field due to high practical values, and numerous theoretical and experimental studies have been conducted to reveal the relationships between the stability of rock masses and their disintegration properties quantitatively. Franklin and Chandra (1972) investigated the process of disintegration under drying and wetting conditions and proposed the first durability test. This was subsequently standardized by both the American Society for Testing and Materials (ASTM 2013) and the International Society for Rock Mechanics (ISRM 2007). The resulting durability index is an important indicator of the disintegration behavior of rocks. Erguler and Ulusay (2009) and Gautam and Shakoor (2016) investigated the difference in the disintegration behavior under laboratory and natural climatic conditions and found that the durability

index of specimens under laboratory conditions is consistent with that under natural climatic conditions. Research performed by Sadisun et al. (2005) and Zhou et al. (2017) pointed out that the durability index, density and compressive strength decreased with an increase in the number of wetting and drying cycles, and the cyclic wetting and drying process is considered to be one of the main processes that can cause degradation and deterioration of rock material.

As for the red-bed soft rock in the drawdown area on bank slopes of landslide, the cyclic drying-wetting process lasts for a long time during the course of reservoir operation and has its own distinct drying-wetting alternating regime (Zhang et al. 2018). Additionally, the disintegration of the red-bed soft rock in the drawdown area is a typical physical and chemical process under cyclic drying-wetting conditions. Although the disintegration of soft rock has attracted extensive attention in previous research, most studies have focused mainly on the disintegration behavior, scarcely any have paid attention to the chemical process of the disintegration and disintegration mechanism (Kyu and Chernov 1998; Sun et al. 2009; Qian et al. 2009). In this study, red-bed argillaceous siltstone were selected to investigate the disintegration characteristics, durability and microstructure characteristics of the red-bed argillaceous siltstone after undergoing various drying-wetting cycles. In the meantime, the evolution of the ion concentration in the aqueous solution during the process of drying-wetting cycles were also analyzed, and the chemical disintegration mechanism of red-bed argillaceous siltstone was comprehensively investigated, which provides theoretical guidance for chemical modification of red-bed landslides in the future.

2 Materials and methods

2.1 Materials

The tested samples with similar close masses, geometric shapes and identical mineral compositions, were red-bed argillaceous siltstone of the Tertiary Wanghudun Formation (E_{1w}). They were collected from Tongcheng, Anhui Province, China. The basic physical properties of the red-bed argillaceous siltstone, including its density, water content, and bulk density, are presented in Table 1. The X-ray diffraction (XRD) results of the samples are testing are illustrated in Fig. 1 and Table 2. It can be observed that the main mineral components of the tested rocks were quartz (44.29%), muscovite (3.97%), calcite (10.47%), albite (17.35%), gypsum (5.09%), and the clay mineral content was 18.82%. In addition, the major chemical components of the tested rock, determined using the X-ray fluorescence (XRF) technique, are listed in Fig. 2. As can be observed, the main chemical components of the tested samples were silicon (Si, 57.82%), aluminum (Al, 16.98%), iron (Fe, 5.21%), sodium (Na, 0.53%), and magnesium (Mg, 3.65%), along with potassium (K, 4.47%) and calcium (Ca, 9.26%).

2.2 Experimental methods

2.2.1 Disintegration experiment

The disintegration experiment, as described by the ASTM and the ISRM, was performed to assess the disintegration behavior of red-bed argillaceous siltstone in the laboratory. In this study, ten cycles were designed and performed to ensure that all the samples completely disintegrated. In general, a single drying-wetting cycle was divided into two processes: drying (from wet to dry state) and wetting (from dry to wet state).

In each cycle, the samples were submerged in deionized water for 24h to wet state and then, removed and dried in an oven at 105℃ for 24 h according to ASTM D4373-14 (2014).

In this study, 20 samples, were selected for the experiments. A total of 10 drying-wetting cycles were carried out for each sample, and the disintegration characteristics of the samples after each cycle was observed and recorded. The disintegration products were sieved by 5, 2, 0.5, and 0.25 mm standard sieves, and the masses and quantities of grains with different particle sizes, were counted after the end of each cycle. The grain-size distribution curves of the disintegration products are useful data for evaluating physical disintegration characteristics of rocks (Czerewko and Cripps 2001; Erguler and Shakoor 2009; Gautam and Shakoor 2013; Zhang et al., 2012; Wu et al. 2010).

2.2.2 Scanning electron microscopy

The samples, subjected to their designated numbers of drying-wetting cycles were broken into small pieces with an approximate size of 5 mm × 5 mm × 5 mm. Pretreatment measures were applied to the samples. First, a hairbrush was used to clean their surface, then they were freeze-dried in an Alpha 1-4 LDplus freeze dryer for 24 h, and finally, vacuum metal spraying technology was used to obtain sufficient conductivity. Morphology observations were simultaneously conducted using a JSM-6490LV scanning electron microscope (SEM) (Devarapalli et al. 2017; Tavanaei and Salehi 2015).

2.2.3 Aqueous solution detection

Different chemical processes can occur during the drying-wetting cycles, which include dissolution/precipitation, ion exchange processes, oxidation, and reduction. Minerals present in rock will partially or completely dissolve in water according to its resistance to chemical weathering. During these chemical interaction processes, the following changes may occur in the system: (1) increase or decrease in the concentration of ions in water, (2) the mobility of the dissolved constituents may be affected (Jalali and Khanlari 2008).

After the samples subjected to the drying-wetting cycles, various ions appeared in the solution, and the concentrations of ions varied with the number of drying-wetting cycles. In this study, the cations and anions were determined in the laboratory after all the samples were filtered using 0.45 μm Millipore membrane filters. The concentration of cations in the solution was measured through inductively coupled plasma mass spectrometry (ICP-MS), and the content of anions was measured using ion chromatography (IC).

All the experiments are performed at an ambient temperature of 20±0.1℃.

3 Experimental results

3.1 Disintegration characteristics

The disintegration characteristics and schematic diagram of samples subjected to different cycles of drying-wetting, were shown in Fig. 3. It can be observed that, in the initial experiment stage, an insignificant variation in the samples could be detected, as cracks appeared only on the edges of the samples and many bubbles formed in the water. With the increases in soaking time, the cracks propagated on the surface of the samples,

177 the sample began to disintegrated, and the disintegration products were mainly fine
178 particles. After experiencing three drying-wetting cycles, obvious disintegration could
179 be observed in the test and the main morphologies of the disintegration products were
180 granular and massive. With the increases in the drying-wetting cycles, an intensified
181 disintegration of the samples could be observed. In the meantime, the number of
182 disintegrated products gradually increased, and the main disintegration product was
183 granular. This result verifies that the red-bed argillaceous siltstone in this study shows
184 a relatively strong disintegration characteristic. The disintegrated process of the red-
185 bed argillaceous siltstone is gradual, and samples is crushed into small fragments, step
186 by step. Water is the most direct influential factor on the disintegration of red-bed
187 argillaceous siltstone, and drying exacerbates the disintegration.

188 **3.2 Particle analysis of disintegration products**

189 The evolution of the grain content with various particle sizes as the drying-wetting
190 cycles increased is presented in Fig. 4.

191 In Fig. 4, it can be observed that the evolutions of particle content of the various
192 particle sizes under the drying-wetting cycles share an inconsistent trend. To be specific,
193 an insignificant variation in the content of particles that are larger than 5 mm could be
194 detected in the initial stage of the experiment, followed by a rapid decrease as the
195 experiment progressed. However, the rate of decrease in the later period gradually
196 slowed down and stabilized, and the content of this particle size was approximately 2%.
197 The evolution trend of the content of particles that are smaller than 0.25 mm is contrary
198 to that of particles that are larger than 5 mm. It remained almost unchanged during the

first three drying–wetting cycles of the samples, which indicates the limited influence of water on the samples at this stage. As the drying-wetting cycles increased to 10, the content of the particles that were smaller than 0.25 mm increased gradually and reached a remarkable value of 83.44%. Additionally, the evolutions of the content of the particles that were 2-5, 0.5-2, and 0.25-0.5 mm in size shared a similar trend, in which an insignificant variation could be recorded in the initial experiment process, followed by an increase as the drying–cycles increased. However, the grain content gradually decreased after reaching a maximum value until the end of the tenth drying–wetting cycle. From these results, it can be concluded that the size of the samples is relatively reduced during the disintegration experiment. Furthermore, the speed of the disintegration of the small particles slowed down until disintegrating stopped. The water-stability of the red-bed argillaceous siltstone increased when its particle size was reduced to less than 2 mm.

3.3 Evaluation of durability

To evaluate the disintegration capacity of the red-bed argillaceous siltstone, and quantify the amount of disintegration, the durability index, proposed by Franklin et al. (1972) and recommended by the ASTM (2004) and the ISRM (2007), was adopted in this paper. As describe by ASTM D4644-14 (2016) and Gamble (1971), the durability index was widely used to evaluate the physical changes and durability of rocks during drying-wetting cycles, and I_{dn} is calculated as the percentage ratio of the final to the initial dry sample weights as follows:

$$I_{dn}=\frac{m_n}{m_0}\times 100\% \quad (1)$$

In Eq. (1), I_{dn} is the durability index after the nth cycle, m_0 is the initial dry weight of the sample, (g), and m_n is the weight of the retained portion of the samples after the nth cycle, (g).

The values of the durability index I_{d1}-I_{d10} obtained from different cycles, are plotted in Fig. 5. As can be observed, I_{d1}-I_{d10} display a negative linear relationship with the number of cycles, and the values of the durability index gradually decrease with an increasing number of drying-wetting cycles. To describe durability index evolutions with the increasing number of drying-wetting cycles, a linear function is employed to fit the experimental data and the best fitting equation is obtained as follows:

$$I_{dn}=112.28-10.09n \quad (2)$$

The fitting result of the evolutions of the durability index with an increase in the number of drying-wetting cycles is illustrated in Fig. 5. The obtained exponential function fits well with the experimental data, and R^2 is 0.986. As the drying-wetting cycles increases, the durability index of the red-bed argillaceous siltstone decreases progressively. Specifically, the values of the durability index (I_d) slowly changed in the first and second cycles, notably decreased from the third cycle to the eighth cycle and varied insignificantly after the eighth cycle. Finally, when the number of drying-wetting cycles increased up to 10, the durability index reaches a minimum value of 11.57. Furthermore, according to the classification system from Franklin et al. (1972) and Zhu et al. (2019), the values of durability obtained in this study indicate that the durability of red-bed argillaceous siltstone is very low.

3.4 Microstructure characteristics

243 To monitor the evolution of the microstructure in the tested samples after exposing
244 them to the drying-wetting cycles, SEM at 1000× magnification was used on samples
245 after 0, 1, 3, 5, 7 and 10 cycles. The results are presented in Fig. 6.

246 Fig. 6(a) shows the initial microstructure characteristics of the tested sample.
247 Before experiencing drying-wetting cycles, the sample had a dense structure, with few
248 flaky aggregates and pores distributed on the surface. After experiencing one drying-
249 wetting cycle, newly formed cracks could be occasionally observed, and the surface of
250 tested sample became rough, as shown in Fig. 6(b). An increase in the drying-wetting
251 cycles caused micro-crack propagation and typically a wider micro-crack distribution
252 in the samples, as shown in Fig. 6(c). After experiencing three drying-wetting cycles,
253 the number of pores and cracks gradually increased. Additionally, flaky aggregates
254 appeared in the sample due to the softening of water. After fifth drying-wetting cycles,
255 the cracks on the surface continued to develop, and the flaky aggregations were
256 adsorbed on the surface with unevenly distributed pores, as shown in Fig. 6(d). After
257 experiencing seven drying-wetting cycles, some clay minerals disaggregated, the flaky
258 aggregations decreased with the appearance of fresh surfaces, as well as the surface
259 began to be relatively smooth again, as shown in Fig. 6(e). Finally, when the number of
260 drying-wetting cycles increased up to 10, as shown in Fig. 6(f), the clay mineral
261 continuously dissolved, the flaky aggregations peel off, and the surface became
262 smoother under the water-rock interaction.

263 As mentioned above, structures in the red-bed argillaceous siltstone, including
264 pores and cracks, notable changed under cyclic drying-wetting conditions. It can be

observed in Fig. 6(a) that, the initial microstructure of the red-bed argillaceous siltstone had a dense structure, with few flaky aggregates and pores distributed on the surface. With the increasing number of drying-wetting cycles, the size and distribution of pores and cracks gradually increased, flaky aggregates appeared in the surface of tested sample due to the softening of water, and the sample became rougher than initial state, as shown in Figs. 6(b)-(d). During the process from the fifth to tenth drying-wetting cycles, the cracks continuously expand under interaction of the water-rock, flaky aggregations peel off and a fresh surface becomes exposed on the surface of sample, as shown in Figs. 6(e) and (f).

3.5 Evolution of ions concentration

Fig. 7 presents the evolution of cations concentration in the aqueous solution during the drying-wetting cycles. The concentration of cations in the solution significantly changed with the increase in the drying-wetting cycles. In the initial stage of the drying-wetting cycles, the concentrations of Na^+ and Ca^{2+} showed notable increases, and the growth trend of Na^+ was higher than that of Ca^{2+}. When the number of drying-wetting cycles reached 3, the concentration of Na^+ reached its maximum value of 12.38mg/L, and then gradually decreased. The concentration of Ca^{2+} reached its maximum value of 4.43mg/L after the seventh drying-wetting cycle and then remained unchanged until the end of the experiment. With an increase in the number of drying-wetting cycles, the concentration of K^+ and Mg^{2+} also increased slightly, whereas the concentration of Al^{3+} remained basically unchanged.

In addition, the evolution of anions concentration in the aqueous solution during

287 the process of drying-wetting cycles were presented in Fig. 8. As shown in Fig. 8, the
288 concentration of anions in the solution changed significantly with an increase in the
289 number of drying-wetting cycles. In which, the changes of SO_4^{2-} and SiO_3^{2-} being
290 more obvious than those in Cl^-. In the initial stage of the drying-wetting cycle, the
291 concentration of SO_4^{2-} and SiO_3^{2-} significantly increased and reached the maximum
292 value in the third drying-wetting cycle. Subsequently, the concentration gradually
293 decreased and became stable. Additionally, small amounts of Cl^- were also detected
294 in the aqueous solution, and the concentration remained almost unchanged during the
295 entire drying-wetting cycle.

296 The results in Figs. 7 and 8 shows that the released concentrations of Na^+, Ca^{2+},
297 SO_4^{2-} and SiO_3^{2-} in the solution were higher than those of Al^{3+}, K^+, Mg^{2+} and Cl^-, imply
298 that the reaction ability of different minerals with water was different. Which is due to
299 the fact that Na^+, Ca^{2+}, SO_4^{2-} and SiO_3^{2-} are active components in ion exchange and
300 adsorption, whereas Al^{3+}, K^+, Mg^{2+} and Cl^- usually exist in stable compound states. For
301 Na^+, Ca^{2+}, SO_4^{2-} and SiO_3^{2-} in the aqueous solution, it is mainly generated from the
302 dissolution of calcite, albite, gypsum, montmorillonite and kaolinite, which causes a
303 large amount of ions to enter into the soak solution, the chemical reactions are shown
304 in Eqs. (3) to (7) (Zhou et al. 2004; Inglezakis, 2005; Xu et al. 2008). After the third
305 drying-wetting cycles, the Na^+ and SO_4^{2-} content decreases continuously, which may
306 be caused by the ex-change adsorption of Na^+ and formation of $CaSO_4$, which can be
307 expressed as Eqs. (8) and (9). In addition, K^+ and Mg^{2+} is an important component of
308 illite, illite has weaker hydrophilicity and ion-exchange adsorption capacity compared

with montmorillonite, and results in a very low content of K^+ and Mg^{2+}. The Al^{3+} and Cl^- are important components of insoluble minerals, usually in a relatively stable compound, therefore, the content of Al^{3+} and Cl^- in the soak solution is low with no obvious change.

$$CaSO_4 \rightarrow Ca^{2+} + SO_4^{2+} \quad (3)$$

$$CaCO_3 + H_2O + CO_2\uparrow \rightarrow Ca^{2+} + 2HCO_3^- \quad (4)$$

$$2NaAlSi_3O_8 + 11H_2O + 2CO_2\uparrow \rightarrow Al_2Si_2O_5(OH)_4 + 2Na^+ + 2HCO_3^- + 4H_2SiO_4^{2-} \quad (5)$$

$$Na_{0.33}Al_{2.33}Si_{3.67}O_{10}(OH)_2 + 12H_20 \rightarrow 0.33Na^+ + 2.33Al(OH)_4^- + 4H_4SiO_4 + 2H^+ \quad (6)$$

$$K_{0.6}Mg_{0.25}Al_{2.3}Si_{3.5}O_{10}(OH)_2 + 11.2H_2O \rightarrow 0.6K^+ + 0.25Mg^{2+} + 2.3Al(OH)_4^- + H_4SiO_4 + 1.2H^+ \quad (7)$$

$$Na^+(l) + Ca^{2+}(s) \rightarrow Na^+(s) + Ca^{2+}(l) \quad (8)$$

$$Ca^{2+} + SO_4^{2+} \rightarrow CaSO_4\downarrow \quad (9)$$

4 Discussion

As mentioned previously, the intact samples gradually disintegrated, and the content of disintegration products with different particle sizes drastically changed, during the experimental process. With the increasing number of drying-wetting cycles, the size and distribution of cracks and pores in the microstructure of sample gradually increased, the surface of sample was no longer dense and uniform. Furthermore, according to the results obtained by XRD, presented in Fig. 1 and Table 2, the red-bed argillaceous siltstone analyzed in this study contains many soluble minerals and clay minerals, mainly include calcite, albite, gypsum, montmorillonite and kaolinite, which easily reacts with deionized water, then dissolves and disperses into the aqueous solution, as schematically shown in Fig. 9. Meantime, the expansion force generated from dissolution process is greater than the attraction between adjacent layers, which

exacerbates the disintegration of intact rock mass, as reported by Lin et al. (2005), Aja (2020), and Min et al. (2016). From these results, it is concluded that the disintegration of red-bed argillaceous siltstone in this study mainly be affected in two stages: water-absorption during wetting and dehydration shrinkage during drying.

During the wetting procedure, the water-absorption of red-bed argillaceous siltstone is mainly related to soluble minerals and clay minerals. When the red-bed argillaceous siltstone contacts with water, the water can interact with minerals through the pores and fissures. With the soluble minerals and clay minerals absorbing water, not only causes the dissolution of soluble minerals and the expansion of clay minerals, but also generates capillary forces which causes the internal cracks to further expand and disintegrate into small particles. Furthermore, after the disintegration caused by the water-absorption, the structure of samples become weakens and softens. During the drying process, the increases in temperature accelerate the previously wetted samples lose water, which further destroy the structure of samples, and increase the rate of disintegration. With the increasing number of drying-wetting cycles, the sample continuously absorb water and lose water, which aggravates the losses of minerals, increases the surface pores and cracks of the sample, and makes the sample gradually disintegrate. Thus, the disintegration of red-bed argillaceous siltstone is the result of the synergistic effect of water and temperature, under drying-wetting cyclic conditions. In the stage of water absorption, the dissolution of minerals and the change of microstructure destroy the stability of the sample structure, which promotes the disintegration of the sample. In the stage of water loss, the increases in temperature and

354 the dehydration shrinkage of sample accelerate the disintegration of red bed
355 argillaceous siltstone.

356 **5 Conclusions**

357 To better understand the disintegration behavior of red bed soft rock, the
358 disintegration characteristics, durability, microstructural characteristics and ions
359 concentration evolution of red-bed argillaceous siltstone under drying-wetting cyclic
360 conditions were investigated in this study. The main conclusions are as follows:

361 (1) The disintegration process of this red-bed argillaceous siltstone during the
362 wetting cycle is gradual, the samples is gradually crushed, and large particles gradually
363 transform into small particles. The drying process exacerbates disintegration. The
364 particle content of disintegration products with different particle sizes significantly
365 changed during the process of drying-wetting cycles.

366 (2) The durability index (I_d) of the red-bed argillaceous siltstone displays a
367 negative linear relationship with the number of cycles, and after experiencing tenth
368 drying-wetting cycles, the values of the durability index reaches a minimum value of
369 11.57, it means that the durability of red-bed argillaceous siltstone is very low.

370 (3) In the microstructural analysis, a continuous drying-wetting process results in
371 significant variation in the surface structure of the sample. The sample surface become
372 disordered and complicated, some pores are gradually penetrate or merge into the large
373 pores, and new micro-fractures are generated.

374 (4) The interaction between water and calcite, albite, gypsum, montmorillonite
375 and kaolinite is the most important factor that influences red-bed argillaceous siltstone

disintegration. A notable changed in concentrations of ions in the aqueous solutions during disintegration suggested that continuous dissolution of minerals, results in a large amount of mineral loss under the action of cyclic drying-wetting.

(5) Based on the results obtained from experiments, the disintegration of red-bed argillaceous siltstone is the result of the synergistic effect of water and temperature. The dissolution of minerals and the change of microstructure during wetting destroy the stability of the sample structure, which promotes the disintegration of the sample. The increases in temperature and the dehydration shrinkage of sample during drying accelerate the disintegration of red bed argillaceous siltstone.

Acknowledgements

This research is financially supported by the National Natural Science Foundation of China (grant No. 41672306 and 41877262), the Special Project for Major Science and Technology in Anhui Province (18030801103), the Natural Science Foundation of Anhui Province (1908085QD168).

Declaration of competing interest

The authors declare that they have no known competing financial interests or personal relationships that could have appeared to influence the work reported in this paper.

References

Aja, S.U., 2019. “On the thermodynamic stability of illite and is minerals.” Clays and Clay Minerals. 67(6): 518-536. https://doi.org/10.1007/s42860-019-00044-x.

ASTM. 2004. Annual Book of ASTM Standards 2004: Section 2, Nonferrous Metal

398 Products. Volume 02.05, Metallic and Inorganic Coatings, Metal Powders,
399 Sintered P/M Structural parts. American Society for Testing and Materials.
400 ASTM. 2013. Annual Book of ASTM Standards 04(08): American Society for Testing
401 Materials. PP 1824, ASTM International, West Conshohocken, PA, USA.
402 ASTM D4373-14. 2014. Standard Test Method for Rapid Determination of Carbonate
403 Content of Soils. ASTM International, West Conshohocken, PA, USA.
404 ASTM D4644-16. 2016. Standard Test Method for Slake Durability of Shales and Other
405 Similar Weak Rocks. ASTM International, West Conshohocken, PA, USA.
406 Bryson, L.S., Gomez-Gutierrez, I.C., Hopkins, T.C., 2012. Development of a new
407 durability index for compacted shale. Engineering Geology. 139-140: 66-75.
408 https://doi.org/10.1016/j.enggeo.2012.04.011.
409 Cantón, Y., Sole-Benet, A., Queralt, I., Pini, R., 2001. Weathering of a gypsum-
410 calcareous mudstone under semi-arid environment at Tabernas, SE Spain:
411 laboratory and field-based experimental approaches. Catena, 44(2): 111-132.
412 https://doi.org/10.1016/S0341-8162(00)00153-3.
413 Czerewko, M.A., Cripps, J.C., 2001. Assessing the durability of mudrocks using the
414 modified jar slake index test. Quarterly Journal of Engineering Geology and
415 Hydrogeology. 34(2): 153-163. https://doi.org/10.1144/qjegh.34.2.153.
416 Deng, H.F., Zhou, M.L., Li, J.L., 2016. Creep degradation mechanism by water-rock
417 interaction in the red-layer soft rock. Arabian Journal of Geosciences. 9(12): 601-
418 612. https://doi.org/10.1007/s12517-016-2604-6.
419 Devarapalli, R.S., Islam, A., Faisal, T.F., 2017. Micro-CT and FIB-SEM imaging and

420 pore structure characterization of dolomite rock at multiple scales. Arabian Journal
421 of Geosciences. 10(16): 361-372. https://doi.org/10.1007/s12517-017-3120-z.
422 Dhakal, G., Yoneda, T., Kato, M., 2002. Slake durability and mineralogical properties
423 of some pyroclastic and sedimentary rocks. Engineering Geology. 65(1): 31-45.
424 https://doi.org/10.1016/S0013-7952(01)00101-6.
425 Doostmohammadi, R., Moosavi, M., Mutschler, T., 2009. Influence of cyclic wetting
426 and drying on swelling behavior of mudstone in south west of Iran. Environmental
427 Geology. 58(5): 999-1009. https://doi.org/10.1007/s00254-008-1579-3.
428 Erguler, Z.A., Ulusay, R., 2009. Assessment of physical disintegration characteristics
429 of clay-bearing rocks: Disintegration index test and a new durability classification
430 chart. Engineering Geology. 105(1-2): 11-19. https://doi.org/10.1016/j.enggeo.
431 2008.12.013.
432 Erguler, Z.A., Shakoor, A., 2009. Quantification of Fragment Size Distribution of Clay-
433 Bearing Rocks after Slake Durability Testing. Environmental and Engineering
434 Geoscience. 15(2): 81-89. https://doi.org/10.2113/gseegeosci.15.2.81.
435 Franklin, J.A., Chandra, R., 1972. The slake-durability test. International Journal of
436 Rock Mechanics and Mining Sciences and Geomechanics Abstracts. 9(3): 325-
437 328. https://doi.org/10.1016/0148-9062(72)90001-0.
438 Gamble, J.C., 1971. Durability-plasticity classification of shales and other argillaceous
439 rocks. Ph.D. thesis. University of Illinois.
440 Gautam, T.P., Shakoor, A., 2016. Comparing the slaking of clay-bearing rocks under
441 laboratory conditions to slaking under natural climatic conditions. Rock

442 Mechanics and Rock Engineering. 49(1): 19-31. https://doi.org/10.1007/s00603-
443 015-0729-7.
444 Ghobadi, M.H., Mousavi, S., 2014. The effect of pH and salty solutions on durability
445 of sandstones of the Aghajari Formation in Khouzestan province, southwest of
446 Iran. Arabian Journal of Geosciences. 7(2): 641-653. https://doi.org/10.1007/
447 s12517-012-0741-0.
448 Gökceoğlu, C., Ulusay, R., Sönmez, H., 2000. Factors affecting the durability of
449 selected weak and clay-bearing rocks from Turkey, with particular emphasis on
450 the influence of the number of drying and wetting cycles. Engineering Geology.
451 57(3-4): 215-237. https://doi.org/10.1016/S0013-7952(00)00031-4.
452 Hajdarwish, A., Shakoor, A., Wells, N.A., 2013. Investigating statistical relationships
453 among clay mineralogy, index engineering properties, and shear strength
454 parameters of mudrocks. Engineering Geology. 159: 45-58. https://doi.org/
455 10.1016/j.enggeo.2013.03.016.
456 Hua. W., Dong, S.M., Li, Y.F., Xu, J., Wang, Q., 2015. The influence of cyclic drying-
457 wetting on the fracture toughness of sandstone. International Journal of Rock
458 Mechanics and Mining Sciences. 78: 331-335. https://doi.org/10.1016/j.ijrmms.
459 2015.06.010.
460 Huang K, Xu L, Zha FS, Lu ZT, Chu CF, Yu C. Similar simulation study on
461 displacement and stress changes response to coal mining in Longdong coal mine,
462 China. Quarterly Journal of Engineering Geology and Hydrogeology 2020.
463 Inglezakis, V.J., 2005. The concept of “capacity” in zeolite ion-exchange systems.

464 Journal of Colloid and Interface Science 281(1): 68-79. https://doi.org/10.1016/
465 j.jcis.2004.08.082.
466 ISRM. 2007. The complete ISRM suggested methods for rock characterization, testing
467 and monitoring: 1976-2006. Ulusay R, Hudson JA (Editors). Ankara, Turkey.
468 628pp.
469 Jalali, M., Khanlari, Z.V. 2008. Major ion chemistry of groundwaters in the Damagh
470 area, Hamadan, western Iran. Environ Geol 54, 87–93. https://doi.org/10.1007
471 /s00254-007-0795-6.
472 Kurlenya, M.V., Oparin, V.N., 1996. Scale factor of phenomenon of zonal disintegration
473 of rock, and canonical series of atomic and ionic radii. Journal of Mining Science.
474 32(2): 81-90. https://doi.org/10.1007/BF02046676.
475 Kyu, N.G., Chernov, O.I., 1998. Role of fluid density in initiating oriented failure and
476 disintegration of rock. Journal of Mining Science. 34(5): 414-420. https://doi.org/
477 10.1007/BF02550696.
478 Liang, B., Tan, X.Y., Jiang, L.G., 2016. Effects of freeze-thaw and drying-wetting
479 cycles on slaking characteristics of mudstone. Chin J Geotech Eng. 38(4): 705-
480 711. https://doi.org/10.11779/CJGE201604015.
481 Lin, M.L., Jeng, F.S., Tsai, L.S., 2005. Wetting weakening of tertiary sandstones—
482 microscopic mechanism. Environ Geol. 48(2), 265–275. https://doi.org/10.1007/
483 s00254-005-1318-y.
484 Liu, C.W., Lu, S.L., 2000. Research on mechanism of mudstone degradation and
485 softening in water. Rock and Soil Mechanics. 21(1): 28-31. https://doi.org/

10.3969/j.issn.1000-7598.2000.01.007.

Min, T., Gao, Y., Chen, L., Kang, Q., Tao, W.Q., 2016. Changes in porosity, permeability and surface area during rock dissolution: effects of mineralogical heterogeneity. International Journal of Heat and Mass Transfer. 103: 900-913. https://doi.org/10.1016/j.ijheatmasstransfer.2016.07.043.

Molina, E., Cultrone, G., Sebastián, E., 2011. The pore system of sedimentary rocks as a key factor in the durability of building materials. Engineering Geology. 118(3-4): 110-121. https://doi.org/10.1016/j.enggeo.2011.01.008.

Newman, G.H., 1983. The effect of water chemistry on the laboratory compression and permeability characteristics of some North Sea chalks. Journal of Petroleum Technology. 35(05): 976-980. https://doi.org/10.2118/10203-PA.

Pejon, O.J., Zuquette, L.V., 1997. Swelling weak rocks: Scanning electron microscopy and microprobe analysis. Symposium on Recent Developments in Soil & Pavement Mechanics.

Pham, Q.T., Vales, F., Malinsky, L., 2007. Effects of desaturation-resaturation on mudstone. Physics and Chemistry of the Earth. 32(8-14): 646-655. https://doi.org/10.1016/j.pce.2006.03.012

Phienwej, N., Peiris, N.I.C., Jinye, L., 1995. Slaking and swelling behaviour of sedimentary rocks of the Lam Ta Khong Pumped Storage Project, Thailand//8th ISRM Congress. International Society for Rock Mechanics and Rock Engineering,

Qian, Q.H., Zhou, X.P., Yang, H.Q., Zhang, Y.X., Li, X.H., 2009. Zonal disintegration of surrounding rock mass around the diversion tunnels in Jinping II Hydropower

508 Station, Southwestern China. Theoretical and Applied Fracture Mechanics. 51:
509 129- 138. https://doi.org/10.1016/j.tafmec.2009.04.006.
510 Rincon, O., Shakoor, A., Ocampo, M., 2016. Investigating the reliability of H/V spectral
511 ratio and image entropy for quantifying the degree of disintegration of weak rocks.
512 Engineering geology. 207, 115-128. https://doi.org/10.1016/j.enggeo.2016.04.020
513 Selen, L., Panthi, K.K., Vistnes, G., 2019. An analysis on the slaking and disintegration
514 extent of weak rock mass of the water tunnels for hydropower project using
515 modified slake durability test. Bulletin of Engineering Geology and the
516 Environment. 79(4): 1919-1937. https://doi.org/10.1007/s10064-019-01656-2.
517 Sadisun, I.A., Shimada, H., Ichinose, M., 2005. Study on the physical disintegration
518 characteristics of Subang claystone subjected to a modified slaking index test.
519 Geotechnical and geological engineering. 23(3): 199-218. https://doi.org/10.1007/
520 s10706-003-6112-6.
521 Sun, C.J., Ning, J.G., Tan, Y.L., Li, H.T., 2009. The Study on Zonal Disintegration of
522 Surrounding Rock in Deep Mudstone Roadway under High Stress. Proceedings of
523 2009 International Symposium on Risk Control and Management of Design.
524 Construction and Operation in Underground Engineering. 225-228. https://
525 doi.org/10.1007/s11629-012-2204-1
526 Tavanaei, A., Salehi, S., 2015. Pore, throat, and grain detection for rock SEM images
527 using digital watershed image segmentation algorithm. J Porous Media. 18(5):
528 507-518. https://doi.org/10.1615/JPorMedia.v18.i5.40.
529 Weng, M.C., Li, H.H., 2012. Relationship between the deformation characteristics and

530 microscopic properties of sandstone explored by the bonded-particle model.
531 International Journal of Rock Mechanics and Mining Sciences. 56: 34-43.
532 https://doi.org/10.1016/j.ijrmms.2012.07.003.
533 Wu, D.X., Liu, H.J., Wang, G.Q., 2010. Laboratory experimental study of slaking
534 characteristics of red-bed soft rock. Chinese Journal of Rock Mechanics and
535 Engineering. 29: 4173-4179. https://doi.org/10.11779/CJGE201604015.
536 Xu, D., Zhou, X., Wang, X., 2008. Adsorption and desorption of Ni2+ on Na-
537 montmorillonite: effect of pH, ionic strength, fulvic acid, humic acid and addition
538 sequences. Applied Clay Science 39(3-4): 133-141. https://doi.org/10.1016/
539 j.clay.2007.05.006.
540 Youn, H., Tonon, F., 2010. Effect of air-drying duration on the engineering properties
541 of four clay-bearing rocks in Texas. Engineering Geology. 115(1-2): 58-67.
542 https://doi.org/10.1016/j.enggeo.2010.06.012
543 Zhang, D., Chen, A., Liu, G., 2012. Laboratory investigation of disintegration
544 characteristics of purple mudstone under different hydrothermal conditions.
545 Journal of Mountain Science. 9(1): 127-136. https://doi.org/10.1007/s11629-012-
546 2204-1.
547 Zhang, Z., Liu, W., Cui, Q., 2018. Disintegration characteristics of moderately
548 weathered mudstone in drawdown area of Three Gorges Reservoir, China. Arabian
549 Journal of Geosciences. 11(15): 405-414. https://doi.org/10.1007/s12517-018-
550 3751-8.
551 Zhou, Z.L., Cai, X., Chen, L., 2017. Influence of cyclic wetting and drying on physical

552 and dynamic compressive properties of sandstone. Engineering geology. 220: 1–
553 12. https://doi.org/10.1016/j.enggeo.2017.01.017.
554 Zhu, C., Tao, Z.G., Yang, S., 2019. V shaped gully method for control- ling rockfall on
555 high-steep slopes in China. Bulletin of Engineering Geology and the Environment.
556 78(4): 2731-2747. https://doi.org/10.1007/s10064-018-1269-7.

List of Figures:

List of Tables:

Figures

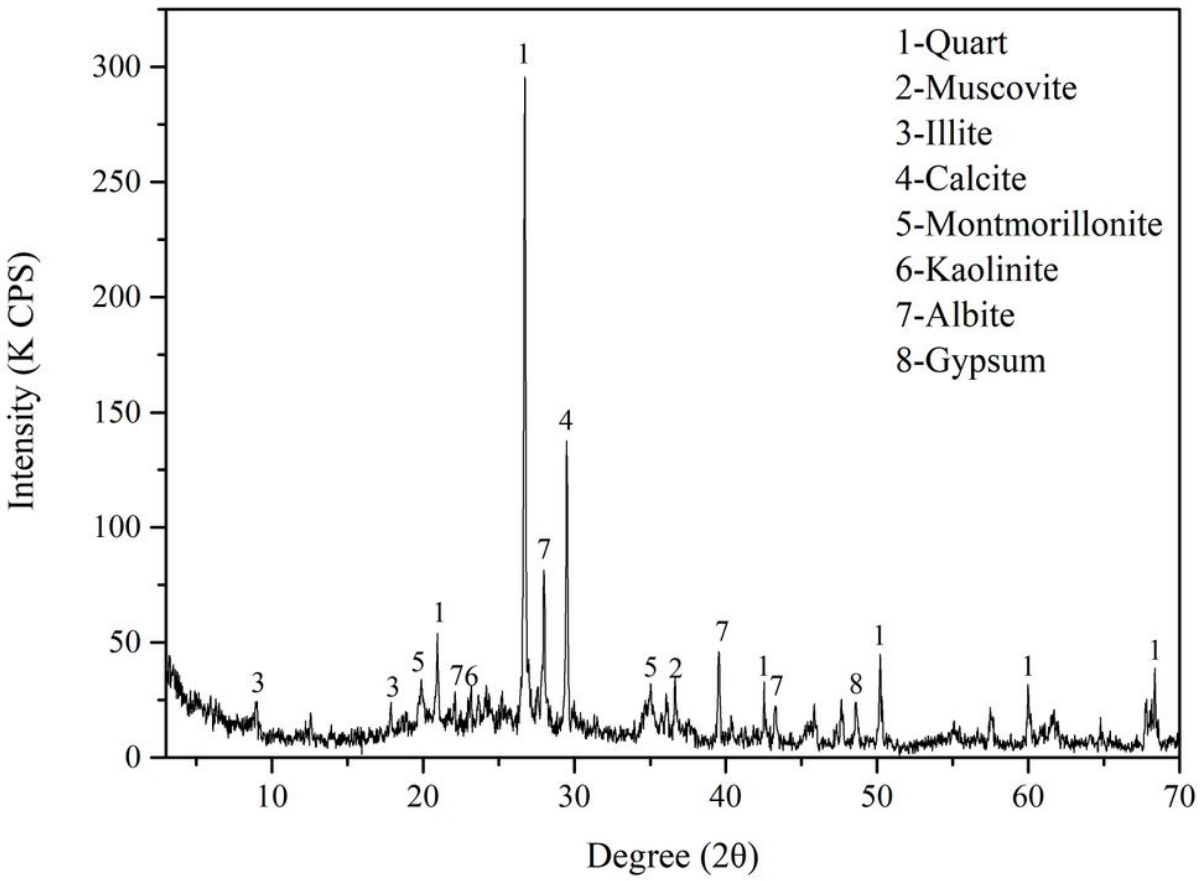

Figure 1

XRD results of tested rock.

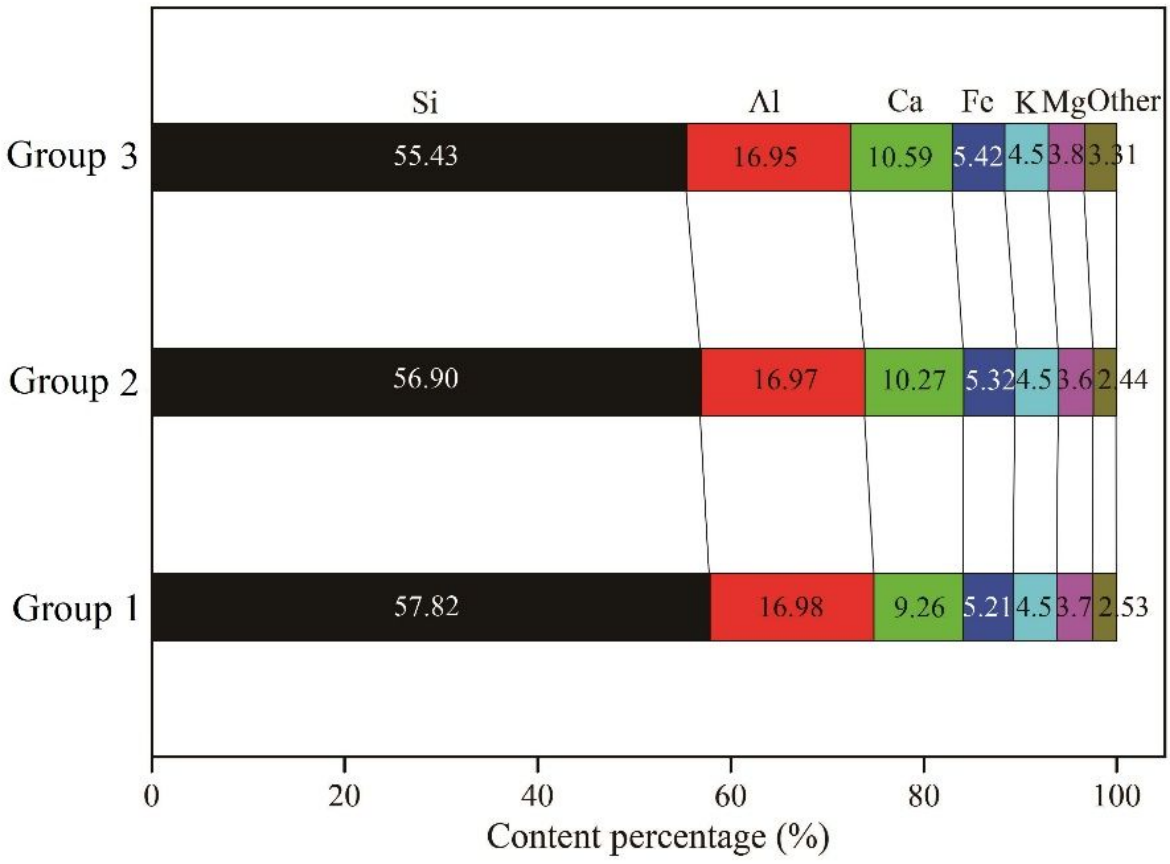

Figure 2

XRF results of tested rock.

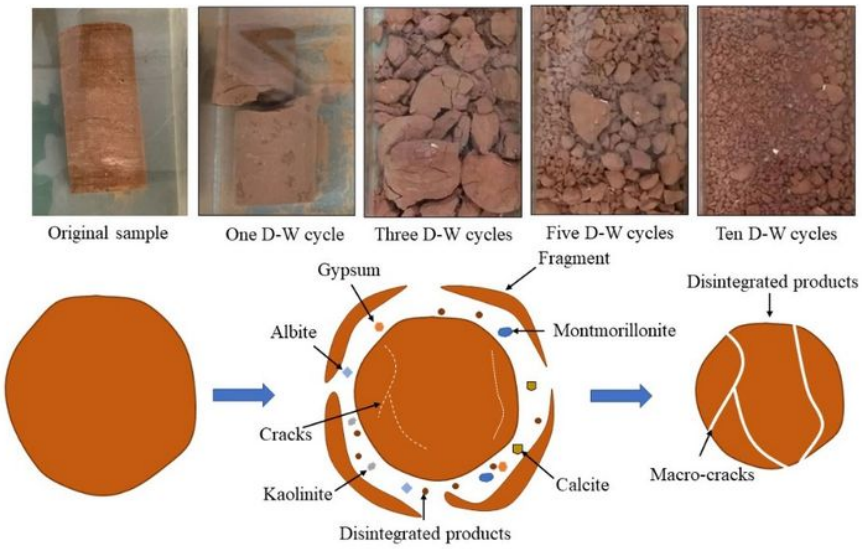

Figure 3

Visible changes in samples subjected to (a) 1 cycle, (b) 3 cycles, (c) 5 cycles, and (d) 10 cycles of drying-wetting.

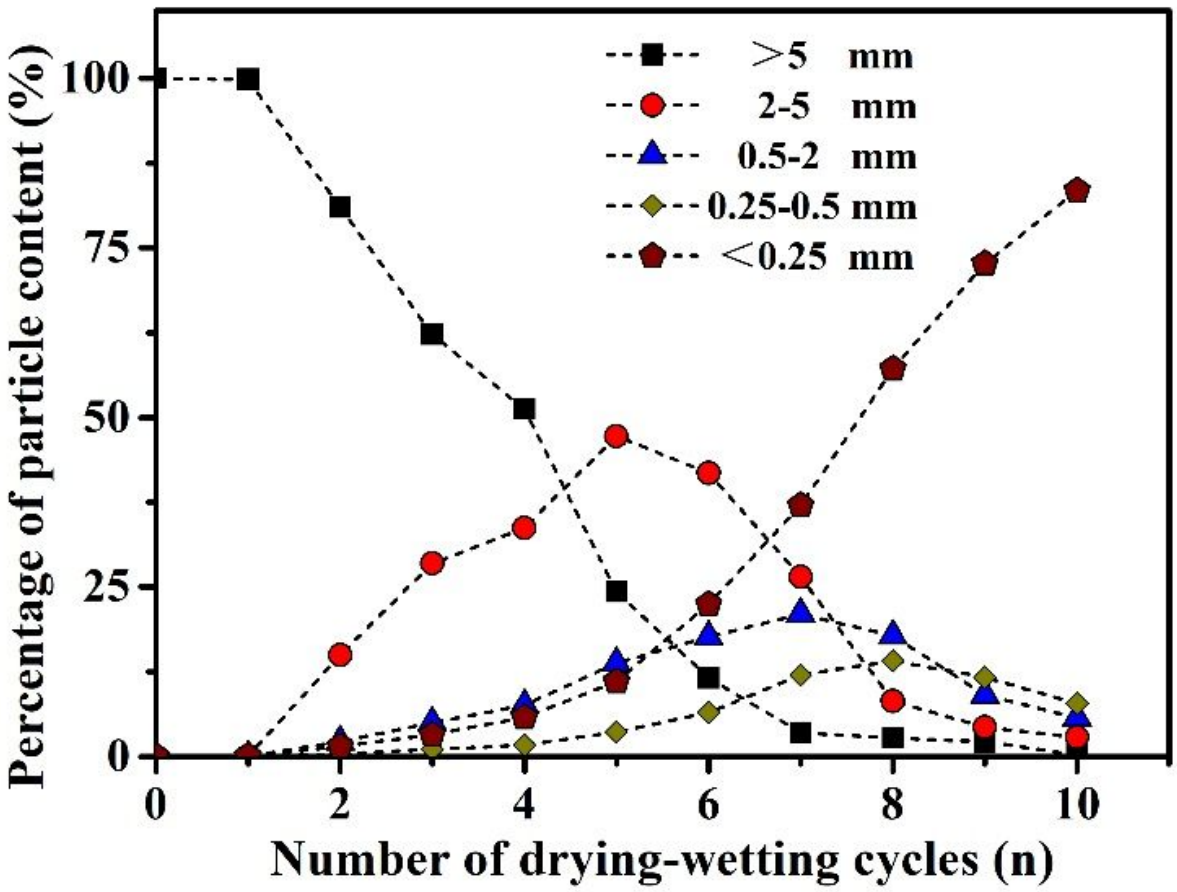

Figure 4

Grain content evolutions of various particle sizes.

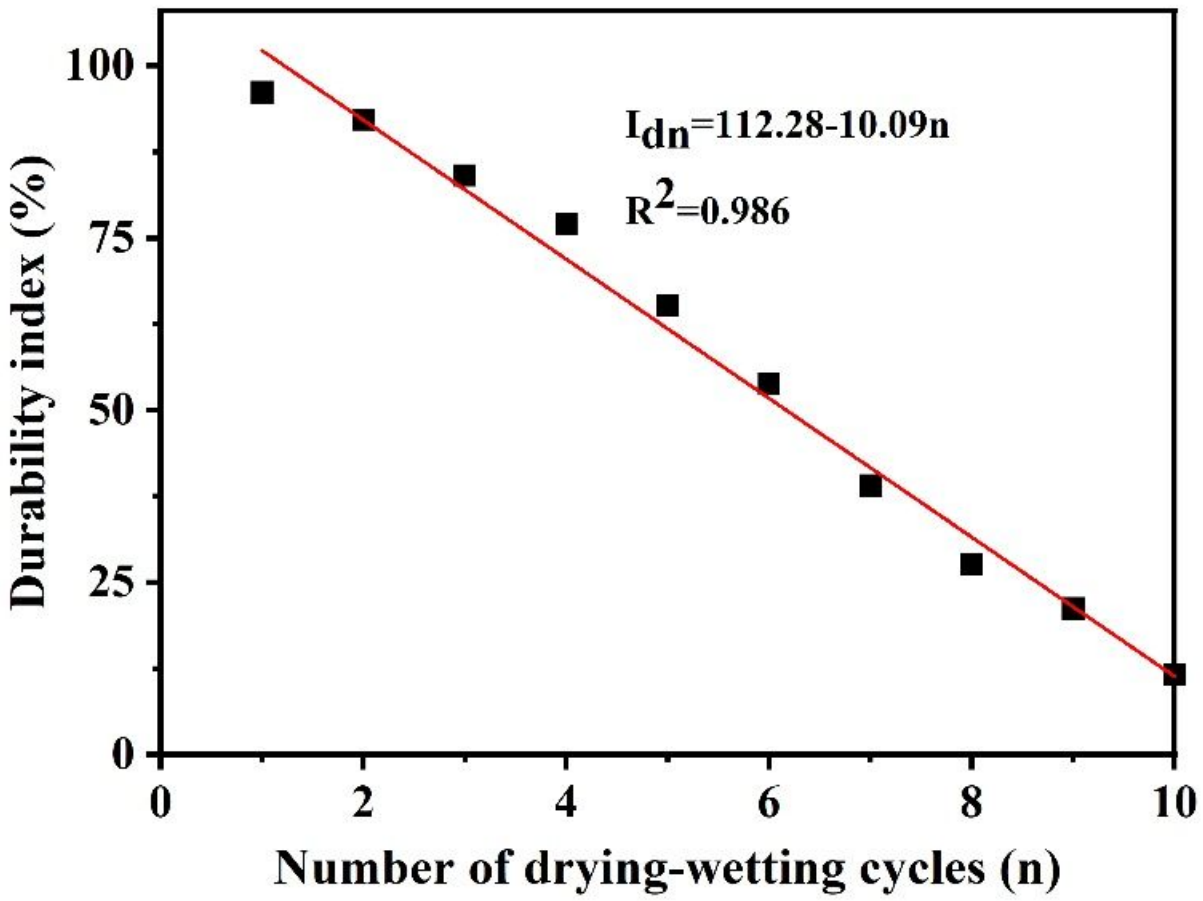

Figure 5

Evolutions of durability Index (Id) with number of drying-wetting cycles.

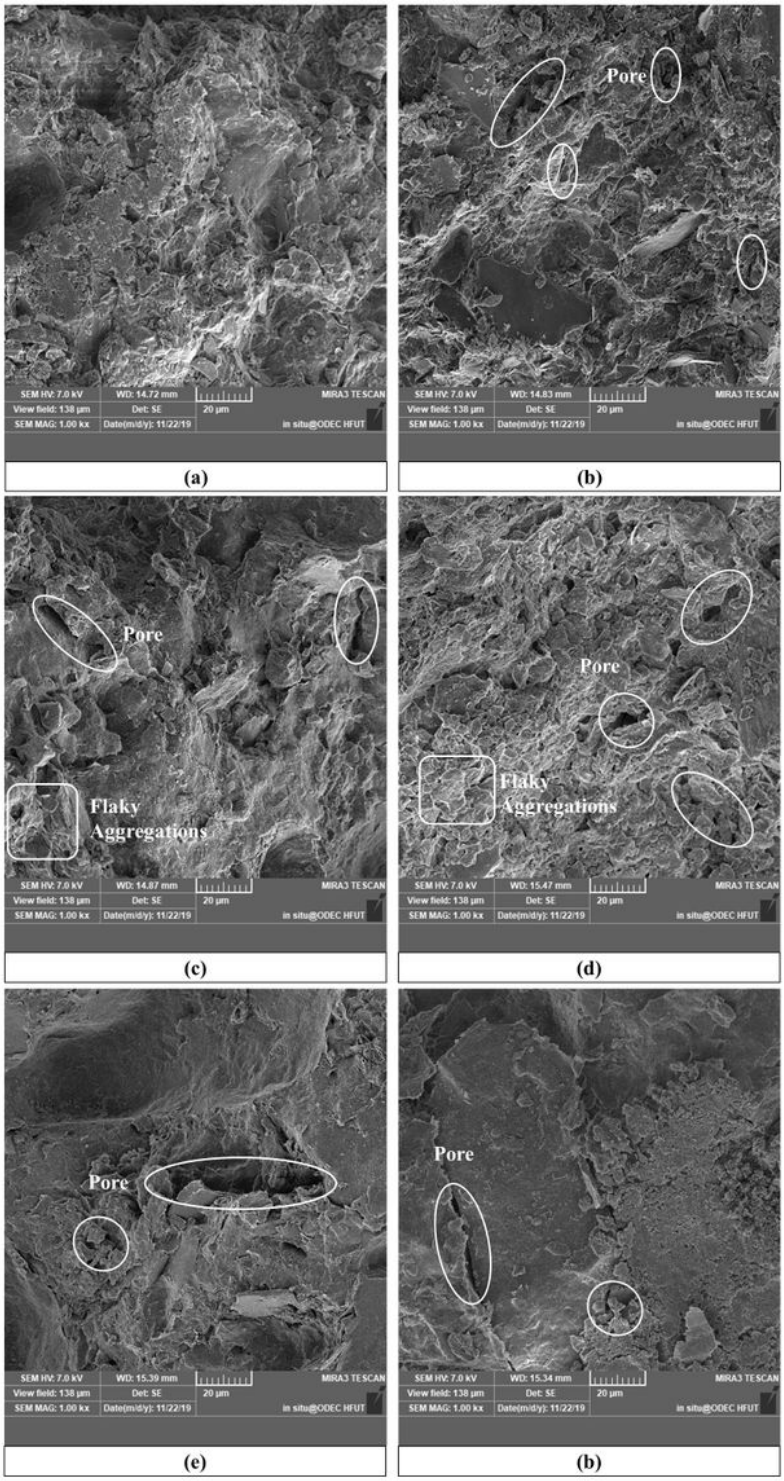

Figure 6

Microstructure characteristics of the tested sample subjected to (a) initial state and after (b) 1 cycles, (c) 3 cycles, (d) 5 cycles, (e) 7 cycles, and (f) 10 cycles of drying-wetting.

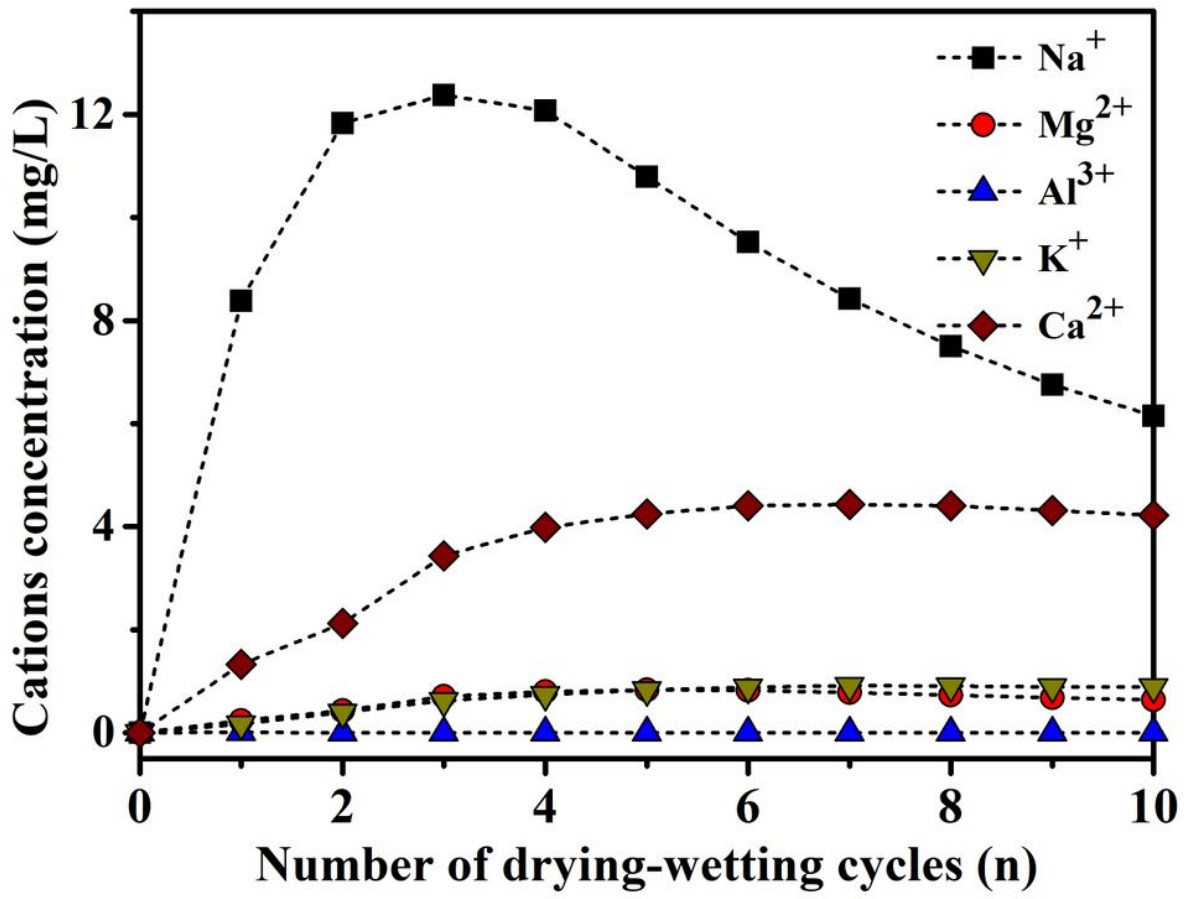

Figure 7

Evolutions of cation concentration in aqueous solution.

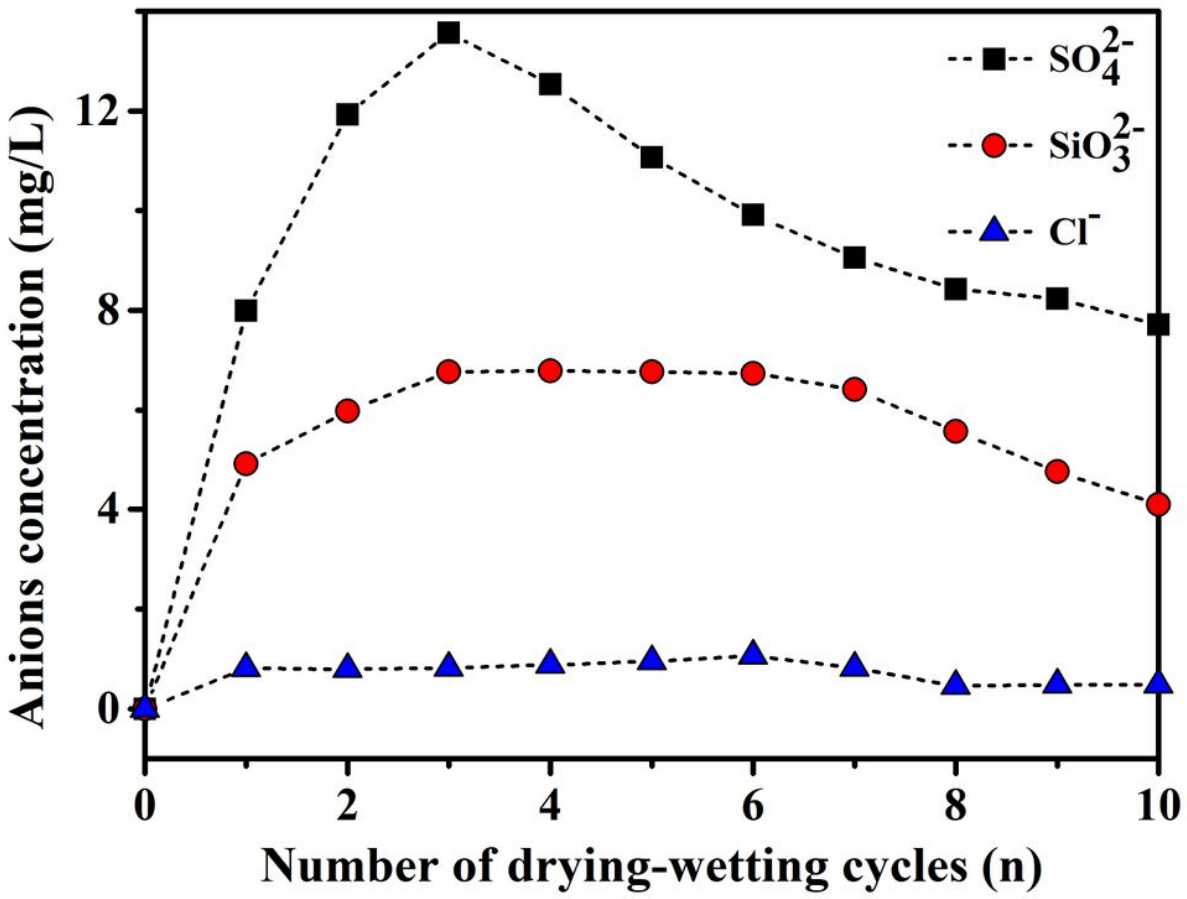

Figure 8

Evolutions of anion concentration in aqueous solution.

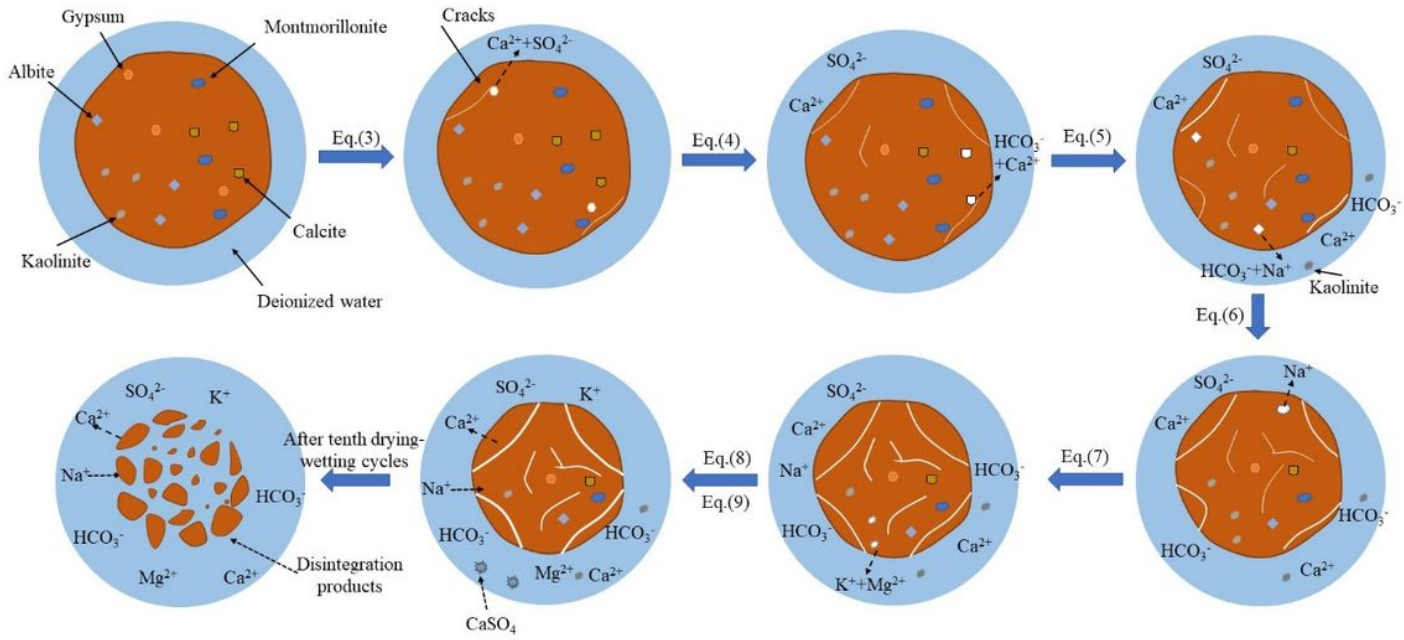

Figure 9

Schematic diagram of chemical water-rock interaction.